

# Search for gravitational waves from Scorpius X-1 with a hidden Markov model in O3 LIGO data with a corrected orbital ephemeris

Andrés F. Vargas<sup>1,2,\*</sup> and Andrew Melatos<sup>1,2</sup>

<sup>1</sup>*School of Physics, University of Melbourne, Parkville, Victoria, 3010, Australia*

<sup>2</sup>*OzGrav-Melbourne, Australian Research Council Centre of Excellence for Gravitational Wave Discovery, Parkville, Victoria, 3010, Australia*

(Dated: October 31, 2023)

Results are presented for a semi-coherent search for gravitational waves from the low-mass X-ray binary Scorpius X-1 in Observing Run 3 (O3) data from the Laser Interferometer Gravitational Wave Observatory, using an updated orbital parameter ephemeris and a hidden Markov model (HMM) to allow for spin wandering. The new orbital ephemeris corrects errors in previously published orbital measurements and implies a new search domain. This search domain does not overlap with the one used in the original Scorpius X-1 HMM O3 search. The corrected domain is approximately three times smaller by area in the  $T_{\text{asc}}-P$  plane than the original domain, where  $T_{\text{asc}}$  and  $P$  denote the time of passage through the ascending node and the orbital period respectively, reducing the trials factor and computing time. No evidence is found for gravitational radiation in the search band from 60 Hz to 500 Hz. Upper limits are computed for the characteristic gravitational wave strain. They are consistent with the values from the original Scorpius X-1 HMM O3 search.

## I. INTRODUCTION

Low-mass X-ray binaries (LMXBs) are targets of numerous gravitational wave searches [1–8]. They are postulated to radiate continuous wave (CW) signals while in a state of rotational equilibrium, where the accretion torque balances the gravitational radiation reaction torque [9–12]. X-ray bright LMXBs are particularly promising targets for CW searches, because the characteristic wave strain  $h_0$ , assuming torque balance, is proportional to the square root of the X-ray flux  $F_X$ . The brightest LMXB is Scorpius X-1 (Sco X-1), whose long-term average X-ray flux is measured at  $F_X = 3.9 \times 10^{-7} \text{ erg cm}^{-2}\text{s}^{-1}$  [13].

Sco X-1 has been a regular target of CW searches with data from the Laser Interferometer Gravitational-Wave Observatory (LIGO) first (O1) [14–16], second (O2) [2, 4], and third (O3) [6–8, 17] observing runs. Although no direct evidence of gravitational radiation has been detected, astrophysically interesting upper limits on  $h_0$  have been obtained. For O3, a hidden Markov model (HMM) pipeline [6, 18] obtained an upper limit at 95% confidence of  $h_0^{95\%} \lesssim 6 \times 10^{-26}$ , assuming circular polarization, across the 100–200 Hz band. For the same frequency band, a cross-correlation (CrossCorr) pipeline [7, 19, 20] obtained  $h_0^{95\%} \lesssim 4 \times 10^{-26}$ , assuming the same polarization.

Searching for CW signals from Sco X-1 presents three challenges: (i) its spin frequency  $f_\star$  (which is related to the CW frequency) is unknown, as the system does not exhibit X-ray pulsations [12, 13]; (ii)  $f_\star$  may wander stochastically due to fluctuations in the hydromagnetic accretion torque [13, 21]; and (iii) the signal model requires precise measurements of the orbital elements: the

projected semimajor axis  $a_0$ , the time of passage through the ascending node  $T_{\text{asc}}$ , and the orbital period  $P$ . The HMM and CrossCorr pipelines are both impacted by (iii). Previous CW searches for Sco X-1 have utilized orbital elements from the campaign of electromagnetic observations known as “Precision Ephemerides for Gravitational-Wave Searches” (PEGS) [22–24] to define the astrophysically motivated parameter domain of the search. The latest update, PEGS IV [24], offers a refined ephemeris and corrects errors in the orbital elements measured by PEGS I [22] and III [23]<sup>1</sup>. Notably, the  $T_{\text{asc}}-P$  domain from PEGS III, used in the O2 [2, 4] and O3 analyses [6, 7], does not overlap with the domain from PEGS IV. A revised Sco X-1 HMM search, using O3 LIGO data [26] and the new PEGS IV ephemeris, is necessary and forms the subject of this paper.

The outline of the paper is as follows. Section II discusses briefly the differences in the measurements and results between PEGS III and PEGS IV. Section III summarizes the HMM search pipeline and the parameter domain. Sections IV and V present the re-analysis output and revised upper limits, respectively. Section VI presents the conclusion.

## II. ORBITAL ELEMENTS

An LMXB emits a quasimonochromatic CW signal [27, 28], which is Doppler-modulated by the relative motion of the source and the detector. The Doppler modulation depends on the sky position (right ascension  $\alpha$ , declination  $\delta$ ) and orbital elements of the binary. Accurate electromagnetic measurements of  $\alpha, \delta, a_0, T_{\text{asc}}$ , and  $P$  reduce the computational cost and trials factor of the search,

\* afvargas@student.unimelb.edu.au

<sup>1</sup> PEGS II [25] targeted Cygnus X-2 instead of Sco X-1.

thereby increasing its sensitivity at a fixed false alarm probability.

For Sco X-1, the sky position is known with microarc-second precision [14, 29]. The orbital eccentricity,  $e$ , satisfies  $e \leq 0.0132$  [24] and is set to zero by assumption in this paper and previous searches [2, 6]. The other orbital elements, i.e.  $a_0$ ,  $T_{\text{asc}}$ , and  $P$ , are harder to measure because of the high accretion rate. The PEGS program tracks the orbital motion via the emission lines generated by Bowen fluorescence of the irradiated donor star [23, 24, 30]. The orbital elements are inferred by fitting a Keplerian orbit ( $e = 0$ ; see Equation (1) in Ref. [23]) to the modulated radial velocities of the Bowen emission lines. The semimajor axis  $a_0$  is related to the orbital speed  $K_1$ , inferred from the Keplerian fit, by  $a_0 = K_1 P / (2\pi)$ . PEGS III obtains  $40 \text{ km s}^{-1} \leq K_1 \leq 90 \text{ km s}^{-1}$ , or equivalently  $1.45 \text{ lt-s} \leq a_0 \leq 3.25 \text{ lt-s}$  [23]. The orbital phase, determined by  $T_{\text{asc}}$  and  $P$ , is dominated by uncertainties related to time-referencing, and the covariance  $\text{cov}(P, T_{\text{asc}})$ . The former refers to possible errors in the barycentric time, for example, while the latter refers to the covariance of the parameters inherent to the Keplerian fit.

The PEGS IV ephemeris [24] improves on previously published PEGS updates [22–24]. PEGS IV is derived from over 20 yr of high-quality spectroscopic observations from the Visual Echelle Spectrograph mounted on the Very Large Telescope. The data, which consist of optical spectra of Bowen emission lines, are analyzed with a new Bayesian approach which supersedes the least-square fit in PEGS III, accounts for observational systematics, and maximizes the precision of the uncertainty estimates [24]. The Bayesian re-analysis reveals two calibration errors in previous ephemerides. First, PEGS I and III do not correct for the mid-exposure time, i.e. the mid time of the various spectroscopic observations. Moreover, they do not adjust for the Solar System heliocentre, which induces a systematic  $T_{\text{asc}}$  error of  $\approx 0.6 \text{ ks}$ . Second, the covariances between orbital elements are underestimated by two orders of magnitude in the Keplerian fit [24].

Table I summarizes the values inferred by PEGS III and IV for  $a_0$ ,  $T_{\text{asc}}$  and  $P$ . The discrepancies between  $T_{\text{asc,ref}}$  and  $P$  in the second and third columns are apparent. Henceforth we define  $T_{\text{asc,ref}}$  as the time of ascension corresponding to November 21 23:16:49 UTC 2010 for PEGS III, and March 06 15:07:40 UTC 2014 for PEGS IV.

In general, CW searches propagate the value of  $T_{\text{asc,ref}}$  to an equivalent time of ascension at a later epoch near or within the relevant LIGO observing run. The propagated value is given by  $T_{\text{asc},0} = T_{\text{asc,ref}} + N_{\text{orb}}P$ , independent of  $a_0$ , where  $N_{\text{orb}}$  is an integer number of orbits. For LIGO O3 data, which starts at  $T_{\text{O3},0} = 1\,238\,166\,483$  GPS time,  $T_{\text{asc,ref}}$  is propagated forward by  $N_{\text{orb}} = 3877$  and  $N_{\text{orb}} = 2352$ , when using the PEGS III and PEGS IV ephemerides, respectively. The original uncertainties for  $T_{\text{asc,ref}}$  and  $P$  are also propagated following the same recipe (see Section III B). Fig. 1 shows the result of prop-

TABLE I. Measured orbital elements, for the PEGS III and IV ephemerides. The  $T_{\text{asc,ref}}$  and  $P$  uncertainties correspond to  $\pm 1\sigma$ . The quoted values are taken from the cited references.

Parameter	PEGS III [23]	PEGS IV [24]
$a_0$ (lt-s)	[1.45, 3.25]	[1.45, 3.25]
$T_{\text{asc,ref}}$ (GPS s)	$974433630 \pm 50$	$1078153676 \pm 33$
$P$ (s)	$68023.86 \pm 0.04$	$68023.92 \pm 0.02$

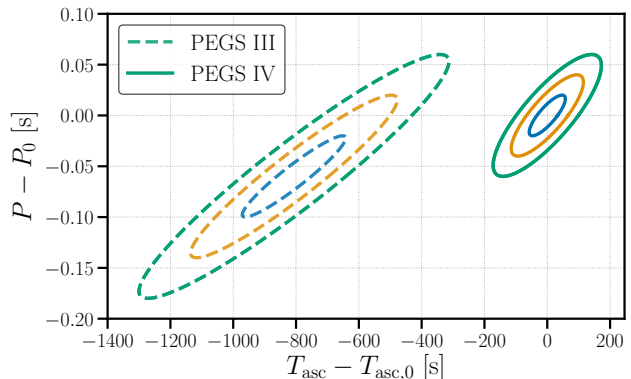


FIG. 1. Forward propagated PEGS III (dashed contours) and PEGS IV (solid contours) uncertainty ellipses corresponding to  $1\sigma$  (blue line),  $2\sigma$  (yellow line), and  $3\sigma$  (green line), for  $T_{\text{asc}}$  and  $P$ . The values of  $T_{\text{asc,ref}}$  (see Table I) are propagated by  $N_{\text{orb}} = 2352$  and  $N_{\text{orb}} = 3877$  to generate the solid and dashed curves, respectively.  $P_0$  represents the central PEGS IV value of  $P$ , i.e.  $P_0 = 68\,023.92 \text{ s}$ , while  $T_{\text{asc},0}$  represents the central PEGS IV value of  $T_{\text{asc,ref}}$  propagated to the start of O3 (dated  $T_{\text{O3},0} = 1\,238\,166\,483$  GPS time), i.e.  $T_{\text{asc},0} = 1\,238\,145\,935.84 \text{ s}$ . The HMM O3 search in this paper covers the region enclosed by the solid green contour.

agating  $T_{\text{asc,ref}}$  and its uncertainties for the PEGS III (dotted contours) and IV (solid contours) ephemerides. The  $T_{\text{asc}}-P$  domains covered by the two ephemerides do not overlap at the  $3\sigma$  level, with a difference of  $\approx 0.8 \text{ ks}$  in  $T_{\text{asc}}$ . The original O2 and O3 searches [2, 4, 6, 7] covered the PEGS III domain and therefore looked in the wrong place. We rectify this error for the HMM search in this paper, just as Ref. [8] rectifies the error for the CrossCorr search.

### III. SEARCH IMPLEMENTATION

In this section we discuss the practical details of the re-analysis. Section III A briefly presents the HMM search algorithm. Section III B defines the search domain and the orbital template grid. Section III C updates the detection thresholds used in the previous analysis. Section III D reviews briefly the vetoes used in the re-analysis.

### A. HMM

A HMM is characterized by a hidden state variable  $q(t)$ , which takes the discrete values  $\{q_1, \dots, q_{N_Q}\}$ , and an observable state  $o(t)$ , which takes the discrete values  $\{o_1, \dots, o_{q_{N_Q}}\}$ . The HMM tracks a stochastic process which jumps between hidden state values at discrete epochs  $\{t_0, \dots, t_{N_T}\}$ . In this CW application,  $f_*(t)$  is mapped onto  $q(t)$ , to track the wandering CW emission frequency from one time step to the next. The probability to jump from  $q_i$  at  $t_n$  to  $q_j$  at  $t_{n+1}$  is given by the transition matrix  $A_{q_j q_i}$  [6]. The transitions are modeled as an unbiased random walk, in which  $f_*(t)$  jumps by  $-1, 0$ , or  $1$  frequency bins, of width  $\Delta f_{\text{drift}}$ , with equal probability at each epoch.

The Fourier transform of the time-domain O3 data maps onto the observable states. The O3 data, with duration  $T_{\text{obs}}$ , is divided into  $N_T$  segments of duration  $T_{\text{drift}}$ , viz.  $N_T = \text{floor}(T_{\text{obs}}/T_{\text{drift}})$ . We discuss the choice of  $T_{\text{drift}}$  for this search in Section III B. The emission probability matrix  $L_{o_j q_i}$  relates the observed data between two consecutive epochs,  $\{o(t') | t_j \leq t' \leq t_j + T_{\text{drift}}\}$ , to the occupied hidden state  $q(t_i)$ . We set  $L_{o_j q_i}$  proportional to the  $\mathcal{J}$ -statistic [2, 18], a frequency domain estimator which ingests the search frequency  $f_0$  and the orbital elements  $(a_0, T_{\text{asc}}, P)$  and accounts for the orbital Doppler shift of the CW carrier frequency.

The probability that the hidden state follows some path  $Q = \{q(t_0), \dots, q(t_{N_T})\}$  given the observed data  $O = \{o(t_0), \dots, o(t_{N_T})\}$  is given by

$$P(Q|O) = \Pi_{q(t_0)} \prod_{i=1}^{N_T} L_{o(t_i)q(t_i)} A_{q(t_i)q(t_{i-1})}, \quad (1)$$

where  $\Pi_{q(t_0)}$  is the prior probability (here uniform, with  $\Pi_{q(t_0)} = 1/N_Q$ ) of being in some initial state  $q(t_0)$  at time  $t_0$ . We use the Viterbi algorithm [31] to calculate the path  $Q^*$  that maximizes  $P(Q|O)$  in Equation (1). We use the log-likelihood of the most likely path  $\mathcal{L} = \ln P(Q|O)$ , output by the Viterbi algorithm, as the detection statistic.

The HMM scheme used in this paper is identical to the one used in the original O3 search [6] and Refs. [2, 3, 5, 18, 32]. For a description of the workflow, see Section III C and the flowchart in Fig. 2 in Ref. [6].

### B. Revised signal templates based on PEGS IV ephemeris

The signal templates searched in the PEGS IV re-analysis are not the same as those searched in the original PEGS III analysis. Specifically, the template locations change in  $T_{\text{asc}}$  and  $P$  but not in  $f_0$ ,  $a_0$ , and sky position.

We set  $T_{\text{drift}} = 10$  days,  $\Delta f_{\text{drift}} = 1/(2T_{\text{drift}}) = 5.787037 \times 10^{-7}$  Hz and  $N_T = 36$ . The choice of  $T_{\text{drift}}$  is

motivated astrophysically and historically. It is the characteristic timescale of the random walk in  $f_*(t)$  inferred from the accretion-driven fluctuations in the X-ray flux of Sco X-1 [1, 27, 34]. It also matches the previously published Sco X-1 searches, and hence enables direct comparison between them [1, 2, 6, 14, 15].

The band to be searched, 60–500 Hz, is identical to the original search. It is divided into sub-bands, each of width  $\Delta f_{\text{sub}} = 0.608148$  Hz and containing  $N_f = 2^{20}$  frequency bins. The total number of sub-bands is  $N_{\text{sub}} = \text{ceil}[(500 - 60) \text{ Hz} / \Delta f_{\text{sub}}] = 725$ .

The  $\mathcal{J}$ -statistic depends on the orbital parameters  $(a_0, T_{\text{asc}}, P)$  in addition to the location of the source, described by the right ascension  $\alpha$  and declination  $\delta$ . These parameters have been measured electromagnetically for Sco X-1 [23, 24, 29, 33]. In this re-analysis the template grid remains unchanged from the original analysis except in the  $T_{\text{asc}}-P$  plane [6]. In particular,  $\alpha$ ,  $\delta$ , the orbital inclination angle  $\iota$ , and the  $a_0$  domain, are unchanged. Following Section II, the  $a_0$  domain is defined by the range  $1.45 \leq a_0/(\text{lt-s}) \leq 3.25$ . Equivalently, we express this range as  $\bar{a}_0 \pm 3\sigma_{a_0}$ , with  $\bar{a}_0 = 2.35$  lt-s and  $\sigma_{a_0} = 0.3$  lt-s. The grid spacing for  $a_0$  is discussed in the next paragraph. As explained in Section II, we propagate forward the reference value  $T_{\text{asc,ref}}$  (see Table I) to the start of O3,  $T_{\text{O3},0}$ , by adding an integer number of orbits  $N_{\text{orb}}$ . This yields a central value  $T_{\text{asc},0} = 1\,238\,145\,935.84$  s. The uncertainties on  $T_{\text{asc,ref}}$  are also propagated to the start of O3 via  $\sigma_{T_{\text{asc}}} = [\sigma_{T_{\text{asc,ref}}}^2 + (N_{\text{orb}}\sigma_P)^2]^{1/2}$ . The latter equation yields  $\sigma_{T_{\text{asc}}} = 57$  s for  $\sigma_{T_{\text{asc,ref}}} = 33$  s and  $\sigma_P = 0.02$  s. We summarize the search domain in Table II.

We cover the orbital parameter domain with a rectangular grid spanning  $(\bar{a}_0 \pm 3\sigma_{a_0}, T_{\text{asc},0} \pm 3\sigma_{T_{\text{asc}}}, P_0 \pm 3\sigma_P)$ . We use Equation (71) of Ref. [35] to set the spacing of the grid and the number of grid points  $N_{a_0}$ ,  $N_{T_{\text{asc}}}$ , and  $N_P$ . For this search we adopt a maximum mismatch of  $\mu_{\text{max}} = 0.1$ , as for the original PEGS III search. Table III presents the number of grid points for several selected sub-bands using the PEGS IV ephemeris. As with the original search, we only analyze templates within the  $3\sigma$  uncertainty ellipses (green solid contour in Fig. 1). Covering the updated  $(T_{\text{asc},0} \pm 3\sigma_{T_{\text{asc}}}, P_0 \pm 3\sigma_P)$  domain requires  $\approx 3$  and  $\approx 2$  times fewer  $N_{T_{\text{asc}}}$  and  $N_P$  grid points, respectively, when averaged across all sub-bands. For instance, the 160 Hz sub-band in the original search uses  $N_{T_{\text{asc}}} = 394$  and  $N_P = 12$  (see Table II in Ref. [6]), while this search uses  $N_{T_{\text{asc}}} = 117$  and  $N_P = 6$ . Overall we analyze between  $1.03 \times 10^5$  and  $3.81 \times 10^7$  templates per sub-band, compared to between  $5.71 \times 10^5$  and  $2.88 \times 10^8$  templates for the PEGS III uncertainty ellipses (dashed contours in Fig. 1).

Besides a rectangular grid, as explained above, there are other alternatives for covering the  $T_{\text{asc}}-P$  domain with templates. For example, using sheared period coordinates [36] or lattice-tilling template banks [37].

TABLE II. Search parameters and their ranges. The column headed “EM data” records the availability of electromagnetic measurements drawn from the references in the last column. As written here  $T_{\text{asc}}$  and  $P$ , plus their uncertainties, define a rectangular parameter domain; values without uncertainties are treated as a single template. In the text generally the central values are denoted with the subscript 0, e.g.  $P_0$ , or an overbar, e.g.  $\bar{a}_0$ . The time of ascension  $T_{\text{asc}}$  stands for the value in [24] propagated up to the start of O3, as described in Section II. We only analyze the templates that are enclosed within the propagated  $T_{\text{asc}}-P$  prior ellipses, i.e. the green solid ellipses in Fig. 1; see Section III B for details.

Parameter	Symbol	Search range	EM data	Reference
Right ascension	$\alpha$	16 h 19 m 55.0850 s	Y	[29]
Declination	$\delta$	$-15^\circ 38' 24.9''$	Y	[29]
Orbital inclination angle	$i$	$44 \pm 6^\circ$	Y	[33]
Projected semi-major axis	$a_0$	$2.35 \pm 0.3 \text{ lt-s}$	Y	[23]
Orbital period	$P$	$68\,023.92 \pm 0.02 \text{ s}$	Y	[24]
GPS time of ascension	$T_{\text{asc}}$	$1\,238\,145\,935.84 \pm 57 \text{ s}$	Y	[24]
Frequency	$f$	60 – 500 Hz	N	...

TABLE III. Selected sub-bands and corresponding  $N_{a_0}, N_{T_{\text{asc}}}, N_P$  template counts needed to cover the  $(\bar{a}_0 \pm 3\sigma_{a_0}, T_{\text{asc},0} \pm 3\sigma_{T_{\text{asc}}}, P_0 \pm 3\sigma_P)$  domain, inferred from the parameter space metric with  $\mu_{\text{max}} = 0.1$  [35]. The orbital templates  $N_{a_0} N_{T_{\text{asc}}} N_P$  per sub-band vary by a factor of  $\approx 385$  across the full band 60–500 Hz. Table II in Ref. [6] indicates that  $N_{T_{\text{asc}}}$  and  $N_P$  for PEGS III are  $\approx 3$  and  $\approx 2$  times lower than for PEGS IV respectively.

Sub-band (Hz)	$N_{a_0}$	$N_{T_{\text{asc}}}$	$N_P$
60	767	45	3
160	2031	117	6
260	3296	190	9
360	4560	263	13
500	6331	364	17

### C. Updated detection threshold

A sub-band is flagged as a candidate when the optimal path with highest log-likelihood, denoted  $\max(\mathcal{L})$ , exceeds a threshold  $\mathcal{L}_{\text{th}}$ , corresponding to a user-selected, fixed, false alarm probability. The process to obtain  $\mathcal{L}_{\text{th}}$  in each sub-band, via Monte-Carlo simulations, is described in Section III D of Ref. [6] and Appendix A in Ref. [5].

In general,  $\mathcal{L}_{\text{th}}$  depends on the trials factor associated with each sub-band, i.e.  $N_{\text{tot}} = N_f N_{a_0} N_{\text{bin}}$ , where  $N_{\text{bin}}$  is the number of templates required to cover the  $T_{\text{asc}}-P$  domain per sub-band. The false alarm probability  $\alpha_{N_{\text{tot}}}$  per sub-band is given by

$$\alpha_{N_{\text{tot}}} = 1 - (1 - \alpha)^{N_{\text{tot}}}, \quad (2)$$

where  $\alpha$  is the false alarm probability in a single terminating frequency bin per orbital template. Here we follow previous Sco X-1 HMM searches [2, 6, 15] and adopt  $\alpha_{N_{\text{tot}}} = 0.01$  to avoid excessive follow-up of candidates and facilitate the comparison between searches.

Given that  $N_{\text{bin}}$  is different in this search, we update our thresholds accordingly. Based on the new values of  $N_{\text{tot}}$  per sub-band from Table III, we obtain

$\mathcal{L}(\text{PEGS III}) - \mathcal{L}(\text{PEGS IV}) \approx 5, 6$ , and  $8$  for the minimum, average, and maximum across all sub-bands. The difference varies monotonically across the search band.

### D. Vetoes

All sub-bands with  $\max(\mathcal{L}) > \mathcal{L}_{\text{th}}$  are subjected to a hierarchy of vetoes to distinguish between a non-Gaussian instrumental artifact and a possible astrophysical signal. In this paper, we follow the original O3 HMM search [6] and apply the known lines veto and the single interferometer (IFO) veto. The known lines veto eliminates any candidate overlapping with a narrow-band noise artifact listed in Ref. [38]. The single IFO veto searches for the candidate in both detectors separately to eliminate any candidate caused by a noise artifact present in one of the detectors only. These vetoes have been used extensively in previous HMM searches [2, 3, 5, 6, 15]. They are defined and justified in detail in the latter references.

## IV. RE-ANALYSIS OF LIGO O3 DATA

The re-analysis described in Section III yields 23 candidates that satisfy  $\max(\mathcal{L}) > \mathcal{L}_{\text{th}}$ . From these candidates, the known lines veto eliminates 21, and the single IFO veto eliminates two.

We plot the results of the re-analysis and the veto procedure in Fig. 2. The horizontal axis, for all panels, correspond to the terminating frequency bin of the optimal path,  $q^*(t_{N_T})$ . The vertical axes correspond to the orbital elements:  $a_0$  (left panel),  $T_{\text{asc}} - T_{\text{asc},0}$  (central panel), and  $P - P_0$  (right panel). Candidates eliminated by the known lines veto and the single IFO veto are marked with a red circle and a blue square, respectively.

This re-analysis also gives us an opportunity to check whether the vetoed candidate sub-bands depend on the orbital ephemerides, i.e. see whether sub-bands consistently get flagged as candidates, regardless of the ephemerides we use. With the exception of the 106.78 Hz



sub-band, all other candidate sub-bands were previously flagged in the original O3 analysis. Among these shared sub-bands, those commencing at 64.30 Hz and 82.51 Hz were vetoed in both analyses by the single IFO veto, while the rest are vetoed by the known lines veto.

## V. FREQUENTIST UPPER LIMITS

Historically, HMM Sco X-1 searches [2, 6, 15] use non-candidate sub-bands to set upper limits on the gravitational wave strain detectable at 95% confidence,  $h_0^{95\%}$ . It is important to check by how much — if at all —  $h_0^{95\%}$  changes when moving from the PEGS III to the PEGS IV ephemerides.

Given the different detection thresholds in the PEGS III and PEGS IV ephemerides (see Section III C), we check as a precaution for any changes in  $h_0^{95\%}$  from the original O3 analysis, as presented in Fig 4. of Ref. [6]. To this end, we apply the same frequentist upper limit procedure used in the PEGS III analysis to selected sub-bands starting at 61.27 Hz, 174.14 Hz, 260.31 Hz, 360.43 Hz, and 500 Hz, spaced across the entire search band. Briefly, the upper limit procedure consists of injecting a Sco X-1-like signal, with parameters  $\{h_0, a_0, T_{\text{asc}}, P\}_{\text{inj}}$  and  $|\cos \iota| = 1$ , into a sub-band. The value of  $h_0$  is progressively reduced, while holding  $\{a_0, T_{\text{asc}}, P\}_{\text{inj}}$  constant, until the difference in  $h_0$  between the last detected and non-detected signals is  $\delta h_0 \leq 1 \times 10^{-27}$ . Section V A of Ref. [6] expands on the upper limit procedure.

We find that the re-analysis and the original O3 search exhibit a similar sensitivity. The average difference, across the selected sub-bands, between the PEGS III and IV upper limits is  $\langle \Delta h_0^{95\%} \rangle = \langle h_0^{95\%}(\text{PEGS III}) - h_0^{95\%}(\text{PEGS IV}) \rangle = 1 \times 10^{-27} = \delta h_0$ . The maximum difference between  $h_0^{95\%}(\text{PEGS III})$  and  $h_0^{95\%}(\text{PEGS IV})$  is  $\max(\Delta h_0^{95\%}) \approx 3 \times 10^{-27}$  for the 360.43 Hz sub-band, while the minimum difference is  $\min(\Delta h_0^{95\%}) \approx -1 \times 10^{-27}$  for the 260.31 Hz sub-band.

Given that  $\langle \Delta h_0^{95\%} \rangle \leq \delta h_0$ , we conclude the PEGS III upper limits remain valid and unchanged for this re-analysis. In general, as the  $\Delta h_0^{95\%}$  value suggests, the difference in detection threshold due to the revised  $N_P$  and  $N_{T_{\text{asc}}}$  template numbers yields  $h_0^{95\%}$  values marginally lower across the frequency range when compared to the PEGS III values. Likewise, the CrossCorr PEGS IV search does not update the original O3 search upper limits, depicted in Fig. 6 of Ref. [7], as the re-analysis sensitivity matches the original O3 search [8].

## VI. CONCLUSIONS

In this paper we re-analyze the LIGO O3 data for CW signals from Sco X-1, using a HMM pipeline in tandem with the corrected and refined PEGS IV orbital ephemeris [24]. The revised search closely fol-

lows the original HMM workflow using the PEGS III ephemeris [6], with identical search implementation, vetoes, and upper limits procedure. No candidate survives the hierarchy of vetoes. The upper limits procedure yields  $h_0^{95\%}$  values consistent with those derived from the search using the PEGS III ephemeris. Consequently, the  $h_0^{95\%}$  values presented in Ref. [6] remain valid and unaltered, e.g. we have  $h_0^{95\%} \leq 6 \times 10^{-26}$ , assuming circular polarization, across the 100–200 Hz band. The re-analysis complements the results of the CrossCorr search using the PEGS IV ephemeris [8], which assumes a signal model with a constant  $f_*$  throughout the observation.

The upcoming fourth LIGO-Virgo-KAGRA (LVK) collaboration observing run (O4) will offer a renewed opportunity to search for Sco X-1, taking advantage of the improved sensitivity of the detectors and the improved precision and accuracy of the PEGS IV ephemeris.

## VII. ACKNOWLEDGEMENTS

The authors thank J. B. Carlin, J. T. Whelan, D. Keitel and the members of the LVK continuous waves group for helpful suggestions which improved the manuscript. This research was supported by the Australian Research Council Centre of Excellence for Gravitational Wave Discovery (OzGrav), grant number CE170100004. This work used computational resources of the OzSTAR national facility at Swinburne University of Technology. OzSTAR is funded by Swinburne University of Technology and also the National Collaborative Research Infrastructure Strategy (NCRIS). This material is based upon work supported by NSF’s LIGO Laboratory which is a major facility fully funded by the National Science Foundation.

This research has made use of data or software obtained from the Gravitational Wave Open Science Center<sup>2</sup>, a service of the LIGO Scientific Collaboration, the Virgo Collaboration, and KAGRA. This material is based upon work supported by NSF’s LIGO Laboratory which is a major facility fully funded by the National Science Foundation, as well as the Science and Technology Facilities Council (STFC) of the United Kingdom, the Max-Planck-Society (MPS), and the State of Niedersachsen/Germany for support of the construction of Advanced LIGO and construction and operation of the GEO600 detector. Additional support for Advanced LIGO was provided by the Australian Research Council. Virgo is funded, through the European Gravitational Observatory (EGO), by the French Centre National de Recherche Scientifique (CNRS), the Italian Istituto Nazionale di Fisica Nucleare (INFN) and the Dutch Nikhef, with contributions by institutions from Belgium, Germany, Greece, Hungary, Ireland, Japan, Monaco,

<sup>2</sup> <https://gwosc.org/>

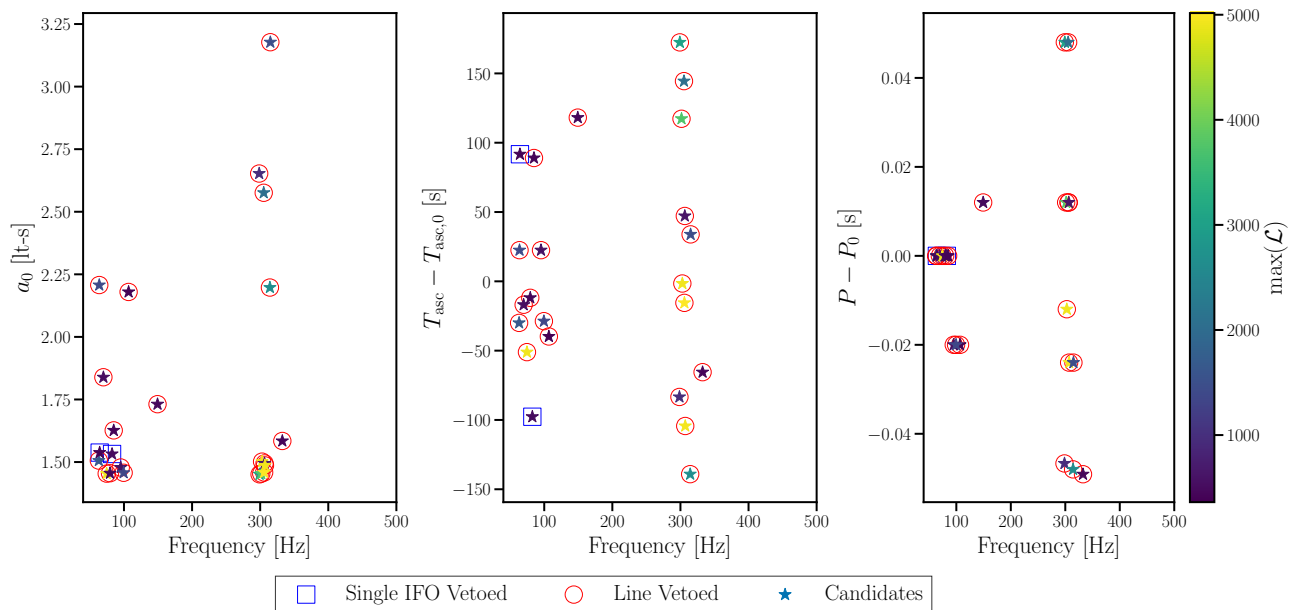


FIG. 2. Candidates (stars) plotted as a function of their terminating frequency bin  $q^*(t_{NT})$  (horizontal axis). The vertical axes feature the orbital parameters:  $a_0$  (left panel), offset from the central time of ascension  $T_{\text{asc}} - T_{\text{asc},0}$  (middle panel), and offset from the central period  $P - P_0$  (right panel). The colour scale corresponds to  $\max(\mathcal{L})$ . Candidates decorated with a red circle or blue square are eliminated by the known lines or single IFO veto, respectively.

Poland, Portugal, Spain. KAGRA is supported by Ministry of Education, Culture, Sports, Science and Technology (MEXT), Japan Society for the Promotion of Science (JSPS) in Japan; National Research Foundation (NRF) and Ministry of Science and ICT (MSIT) in

Korea; Academia Sinica (AS) and National Science and Technology Council (NSTC) in Taiwan.

This work has been assigned LIGO document number P2300322.

- 
- [1] J. Aasi, B. P. Abbott, R. Abbott, T. Abbott, M. R. Abernathy, F. Acernese, K. Ackley, C. Adams, T. Adams, P. Addesso, and et al., Directed search for gravitational waves from Scorpius X-1 with initial LIGO data, *Phys. Rev. D* **91**, 062008 (2015), [arXiv:1412.0605 \[gr-qc\]](#).
  - [2] B. P. Abbott, R. Abbott, T. D. Abbott, S. Abraham, F. Acernese, K. Ackley, C. Adams, R. X. Adhikari, V. B. Adya, C. Affeldt, and et al., Search for gravitational waves from Scorpius X-1 in the second Advanced LIGO observing run with an improved hidden Markov model, *Phys. Rev. D* **100**, 122002 (2019), [arXiv:1906.12040 \[gr-qc\]](#).
  - [3] H. Middleton, P. Clearwater, A. Melatos, and L. Dunn, Search for gravitational waves from five low mass x-ray binaries in the second Advanced LIGO observing run with an improved hidden Markov model, *Phys. Rev. D* **102**, 023006 (2020), [arXiv:2006.06907 \[astro-ph.HE\]](#).
  - [4] Y. Zhang, M. A. Papa, B. Krishnan, and A. L. Watts, Search for Continuous Gravitational Waves from Scorpius X-1 in LIGO O2 Data, *ApJ* **906**, L14 (2021), [arXiv:2011.04414 \[astro-ph.HE\]](#).
  - [5] The LIGO Scientific Collaboration, the Virgo Collaboration, the KAGRA Collaboration, R. Abbott, T. D. Abbott, F. Acernese, K. Ackley, C. Adams, N. Adhikari, R. X. Adhikari, and et al., Search for continuous gravitational waves from 20 accreting millisecond X-ray pulsars in O3 LIGO data, [arXiv:2109.09255 \(2021\)](#), [arXiv:2109.09255 \[astro-ph.HE\]](#).
  - [6] R. Abbott, H. Abe, F. Acernese, K. Ackley, N. Adhikari, R. X. Adhikari, V. K. Adkins, V. B. Adya, C. Affeldt, D. Agarwal, and et al., Search for gravitational waves from Scorpius X-1 with a hidden Markov model in O3 LIGO data, *Phys. Rev. D* **106**, 062002 (2022), [arXiv:2201.10104 \[gr-qc\]](#).
  - [7] R. Abbott, H. Abe, F. Acernese, K. Ackley, S. Adhikari, N. Adhikari, R. X. Adhikari, V. K. Adkins, V. B. Adya, C. Affeldt, and et al., Model-based Cross-correlation Search for Gravitational Waves from the Low-mass X-Ray Binary Scorpius X-1 in LIGO O3 Data, *ApJ* **941**, L30 (2022), [arXiv:2209.02863 \[astro-ph.HE\]](#).
  - [8] J. T. Whelan, R. Tenorio, J. K. Wofford, J. A. Clark, E. J. Daw, E. Goetz, D. Keitel, A. Neunzert, A. M. Sintes, K. J. Wagner, and et al., Search for Gravitational Waves from Scorpius X-1 in LIGO O3 Data with Corrected Orbital Ephemeris, *ApJ* **949**, 117 (2023), [arXiv:2302.10338 \[astro-ph.HE\]](#).
  - [9] J. Papaloizou and J. E. Pringle, Gravitational radiation and the stability of rotating stars., *MNRAS* **184**, 501

TABLE IV. Candidates yielded by the O3 re-analysis. The first and second columns correspond to the starting frequency of the sub-band containing the candidate, and the log-likelihood of the candidate, respectively. The third and fourth columns record the outcome of the two vetoes described in Section III D. Candidates are marked with  $\checkmark$  if they pass the veto or **X** if they do not. H and L correspond to the  $\max(\mathcal{L})$  obtained using Hanford-only and Livingston-only data.

Sub-band (Hz)	$\max(\mathcal{L})/10^3$	Known lines veto	Single IFO veto
63.09	1.65	<b>X</b>	...
63.70	1.41	<b>X</b>	...
64.30	0.38	$\checkmark$	<b>X</b>
69.76	0.52	<b>X</b>	...
74.62	4.93	<b>X</b>	...
79.47	0.43	<b>X</b>	...
82.51	0.49	$\checkmark$	<b>X</b>
84.93	0.40	<b>X</b>	...
95.25	0.57	<b>X</b>	...
99.50	1.34	<b>X</b>	...
106.78	0.36	<b>X</b>	...
149.26	0.46	<b>X</b>	...
298.53	0.95	<b>X</b>	...
299.14	3.02	<b>X</b>	...
301.57	3.73	<b>X</b>	...
302.78	4.91	<b>X</b>	...
305.21	2.05	<b>X</b>	...
305.81	5.01	<b>X</b>	...
306.42	0.61	<b>X</b>	...
307.03	4.94	<b>X</b>	...
314.31	2.63	<b>X</b>	...
314.92	1.47	<b>X</b>	...
332.51	0.43	<b>X</b>	...
Total: 23			

- (1978).
- [10] R. V. Wagoner, Gravitational radiation from accreting neutron stars, *ApJ* **278**, 345 (1984).
- [11] L. Bildsten, Gravitational Radiation and Rotation of Accreting Neutron Stars, *ApJ* **501**, L89 (1998), [arXiv:astro-ph/9804325 \[astro-ph\]](#).
- [12] K. Riles, Gravitational waves: Sources, detectors and searches, *Progress in Particle and Nuclear Physics* **68**, 1 (2013), [arXiv:1209.0667 \[hep-ex\]](#).
- [13] A. L. Watts, B. Krishnan, L. Bildsten, and B. F. Schutz, Detecting gravitational wave emission from the known accreting neutron stars, *MNRAS* **389**, 839 (2008), [arXiv:0803.4097 \[astro-ph\]](#).
- [14] B. P. Abbott, R. Abbott, T. D. Abbott, F. Acernese, K. Ackley, C. Adams, T. Adams, P. Addesso, R. X. Adhikari, V. B. Adya, and et al., Upper Limits on Gravitational Waves from Scorpius X-1 from a Model-based Cross-correlation Search in Advanced LIGO Data, *ApJ* **847**, 47 (2017), [arXiv:1706.03119 \[astro-ph.HE\]](#).
- [15] B. P. Abbott, R. Abbott, T. D. Abbott, F. Acernese, K. Ackley, C. Adams, T. Adams, P. Addesso, R. X. Adhikari, V. B. Adya, and et al., Search for gravitational waves from Scorpius X-1 in the first Advanced LIGO observing run with a hidden Markov model, *Phys. Rev. D* **95**, 122003 (2017), [arXiv:1704.03719 \[gr-qc\]](#).
- [16] B. P. Abbott, R. Abbott, T. D. Abbott, M. R. Abernathy, F. Acernese, K. Ackley, C. Adams, T. Adams, P. Addesso, R. X. Adhikari, and et al., Directional Limits on Persistent Gravitational Waves from Advanced LIGO's First Observing Run, *Phys. Rev. Lett.* **118**, 121102 (2017), [arXiv:1612.02030 \[gr-qc\]](#).
- [17] R. Abbott, T. D. Abbott, S. Abraham, F. Acernese, K. Ackley, A. Adams, C. Adams, R. X. Adhikari, V. B. Adya, C. Affeldt, and et al., Search for anisotropic gravitational-wave backgrounds using data from Advanced LIGO and Advanced Virgo's first three observing runs, *Phys. Rev. D* **104**, 022005 (2021), [arXiv:2103.08520 \[gr-qc\]](#).
- [18] S. Suvorova, P. Clearwater, A. Melatos, L. Sun, W. Moran, and R. J. Evans, Hidden Markov model tracking of continuous gravitational waves from a binary neutron star with wandering spin. II. Binary orbital phase tracking, *Phys. Rev. D* **96**, 102006 (2017), [arXiv:1710.07092 \[astro-ph.IM\]](#).
- [19] S. Dhurandhar, B. Krishnan, H. Mukhopadhyay, and J. T. Whelan, Cross-correlation search for periodic gravitational waves, *Phys. Rev. D* **77**, 082001 (2008), [arXiv:0712.1578 \[gr-qc\]](#).
- [20] J. T. Whelan, S. Sundaresan, Y. Zhang, and P. Peiris, Model-based cross-correlation search for gravitational waves from Scorpius X-1, *Phys. Rev. D* **91**, 102005 (2015), [arXiv:1504.05890 \[gr-qc\]](#).
- [21] M. de Kool and U. Anzer, A simple analysis of period noise in binary X-ray pulsars., *MNRAS* **262**, 726 (1993).
- [22] D. K. Galloway, S. Premachandra, D. Steeghs, T. Marsh, J. Casares, and R. Cornelisse, Precision Ephemerides for Gravitational-wave Searches. I. Sco X-1, *ApJ* **781**, 14 (2014), [arXiv:1311.6246 \[astro-ph.HE\]](#).
- [23] L. Wang, D. Steeghs, D. K. Galloway, T. Marsh, and J. Casares, Precision Ephemerides for Gravitational-wave

- Searches - III. Revised system parameters of Sco X-1, *MNRAS* **478**, 5174 (2018), [arXiv:1806.01418 \[astro-ph.HE\]](#).
- [24] T. L. Killestein, M. Mould, D. Steeghs, J. Casares, D. K. Galloway, and J. T. Whelan, Precision Ephemerides for Gravitational-wave Searches - IV. Corrected and refined ephemeris for Scorpius X-1, *MNRAS* **520**, 5317 (2023), [arXiv:2302.00018 \[astro-ph.HE\]](#).
- [25] S. S. Premachandra, D. K. Galloway, J. Casares, D. T. Steeghs, and T. R. Marsh, Precision Ephemerides for Gravitational Wave Searches. II. Cyg X-2, *ApJ* **823**, 106 (2016), [arXiv:1604.03233 \[astro-ph.HE\]](#).
- [26] R. Abbott, H. Abe, F. Acernese, K. Ackley, S. Adhicary, N. Adhikari, R. X. Adhikari, V. K. Adkins, V. B. Adya, C. Affeldt, and et al., Open Data from the Third Observing Run of LIGO, Virgo, KAGRA, and GEO, *ApJS* **267**, 29 (2023), [arXiv:2302.03676 \[gr-qc\]](#).
- [27] A. Mukherjee, C. Messenger, and K. Riles, Accretion-induced spin-wandering effects on the neutron star in Scorpius X-1: Implications for continuous gravitational wave searches, *Phys. Rev. D* **97**, 043016 (2018), [arXiv:1710.06185 \[gr-qc\]](#).
- [28] R. Tenorio, D. Keitel, and A. M. Sintes, Search Methods for Continuous Gravitational-Wave Signals from Unknown Sources in the Advanced-Detector Era, *Universe* **7**, 474 (2021), [arXiv:2111.12575 \[gr-qc\]](#).
- [29] C. F. Bradshaw, E. B. Fomalont, and B. J. Geldzahler, High-Resolution Parallax Measurements of Scorpius X-1, *ApJ* **512**, L121 (1999).
- [30] D. Steeghs and J. Casares, The Mass Donor of Scorpius X-1 Revealed, *ApJ* **568**, 273 (2002), [arXiv:astro-ph/0107343 \[astro-ph\]](#).
- [31] A. Viterbi, Error bounds for convolutional codes and an asymptotically optimum decoding algorithm, *IEEE Transactions on Information Theory* **13**, 260 (1967).
- [32] A. F. Vargas and A. Melatos, Search for continuous gravitational waves from PSR J 0437 -4715 with a hidden Markov model in O3 LIGO data, *Phys. Rev. D* **107**, 064062 (2023), [arXiv:2208.03932 \[gr-qc\]](#).
- [33] E. B. Fomalont, B. J. Geldzahler, and C. F. Bradshaw, Scorpius X-1: The Evolution and Nature of the Twin Compact Radio Lobes, *ApJ* **558**, 283 (2001), [arXiv:astro-ph/0104372 \[astro-ph\]](#).
- [34] C. Messenger, H. J. Bulten, S. G. Crowder, V. Dergachev, D. K. Galloway, E. Goetz, R. J. G. Jonker, P. D. Lasky, G. D. Meadors, A. Melatos, S. Premachandra, K. Riles, L. Sammut, E. H. Thrane, J. T. Whelan, and Y. Zhang, Gravitational waves from Scorpius X-1: A comparison of search methods and prospects for detection with advanced detectors, *Phys. Rev. D* **92**, 023006 (2015), [arXiv:1504.05889 \[gr-qc\]](#).
- [35] P. Leaci and R. Prix, Directed searches for continuous gravitational waves from binary systems: Parameter-space metrics and optimal Scorpius X-1 sensitivity, *Phys. Rev. D* **91**, 102003 (2015), [arXiv:1502.00914 \[gr-qc\]](#).
- [36] K. J. Wagner, J. T. Whelan, J. K. Wofford, and K. Wette, Template lattices for a cross-correlation search for gravitational waves from Scorpius X-1, *Classical and Quantum Gravity* **39**, 075013 (2022), [arXiv:2106.16142 \[gr-qc\]](#).
- [37] A. Mukherjee, R. Prix, and K. Wette, Implementation of a new WEAVE-based search pipeline for continuous gravitational waves from known binary systems, *Phys. Rev. D* **107**, 062005 (2023), [arXiv:2207.09326 \[gr-qc\]](#).
- [38] E. Goetz, A. Neunzert, K. Riles, A. Matas, S. Kandhasamy, J. Tasson, C. Barschaw, H. Middleton, S. Hughey, L. Mueller, J. Heinzl, J. Carlin, A. Vargas, and I. Hollows, T2100200-v1: O3 lines and combs in found in self-gated C01 data.